論文 / 著書情報
Article / Book Information

Title	Dynamics and Kinetics of Laser-Filament Plasma in Strong External Electric
Authors	Takashi Fujii, Alexei Zhidkov, Megumu Miki, Kiyohiro Sugiyama, Naohiko Goto, Shuzo Eto, Yuji Oishi, Eiki Hotta, Koshichi Nemoto
Citation	Chinese Journal of Physics, Vol. 52, No. 1-II, pp. 440-464
Pub. date	2014, 2

CHINESE JOURNAL OF PHYSICS VOL. 52, NO. 1-II February2014

Review

Dynamics and Kinetics of Laser-Filament Plasma in Strong External Electric Fields and Applications

Takashi Fujii,[1,2,*] Alexei Zhidkov,[1] Megumu Miki,[1] Kiyohiro Sugiyama,[2] Naohiko Goto,[1] Shuzo Eto,[1] Yuji Oishi,[1] Eiki Hotta,[2] and Koshichi Nemoto[1]

[1]*Electric Power Engineering Research Laboratory, Central Research Institute of Electric Power Industry, 2-6-1 Nagasaka, Yokosuka-shi, Kanagawa 240-0196, Japan*

[2]*Interdisciplinary Graduate School of Science and Engineering, Tokyo Institute of Technology, 4259 Nagatsuta-cho, Midori-ku, Yokohama-shi, Kanagawa 226-8502, Japan*

(Received November 13, 2013)

Physics of atmospheric laser-induced filaments in strong electric fields provides us with good instruments for the distant study and control of atmospheric and industrial high voltage discharges and accompanying processes. Dynamics and kinetics of laser filaments in strong non-uniform electric fields are studied both theoretically and experimentally with the high temporal and spatial resolution. Among others, a considerable reduction of the breakdown potential was found and was attributed to a filament-induced leader. Two breakdown modes, fast and slow, were found in 0.4 MV positive dc-voltage discharges activated by filaments. In the fast mode with duration order of a few microseconds, the filament may acquire the electrode potential and temporarily maintain it, becoming a leader. The slow mode with its duration order of 1 ms appears with a considerably smaller voltage reduction when the leader decays before the secondary streamer. Long, about a half of microsecond, non-uniform corona UV burst is observed after the laser-filament plasma appears nearby an electrode biased (positively or negatively) slightly higher than the corona discharge threshold. The effects of electron runaway in positive high-voltage-impulse discharges were studied. Strong hard ($\varepsilon > 100$ keV) x-rays being observed from impulse atmospheric discharges just before the breakdown were completely stopped with the use of the laser-filament plasma. Runaway electrons, generating such x-rays, disappear if the laser-filament plasma is ignited perpendicularly to the runaway nearby the positive electrode. These results are important to understand the filament physics, and also useful for the applications to laser triggered lightning, electric field measurement, protection of high-voltage facility and others.

DOI: 10.6122/CJP.52.440 PACS numbers: 52.38.Hb, 52.80.Mg, 52.25.Tx

I. INTRODUCTION

Recently, the laser filament plasma (LFP) [1–18], produced by intense ultra-short laser pulses, in strong external electric fields has attracted interest both in the physics of

*Electronic address: fujii@criepi.denken.or.jp

streamer discharges [19, 20] and in various applications such as the discharge triggering [21–35], the generation of terahertz radiation [36, 37], and the measurement of electric fields in atmosphere [38–43].

Although atmospheric electricity is a subject of longtime study, there is still no practical use of its huge energy. For example, the extreme event such as lightning is out of human control. For control of lightning, laser-triggered discharge by filaments is of particular interest. However, the physics of laser filaments in strong non-uniform electric fields has yet to be understood. Initially, the laser-triggered discharge using long laser pulses in air has been studied for lightning protection of sensitive installations such as electrical power plants, chemical plants, and airports [44]. Recently, the femtosecond (fs)- pulse-laser-triggered discharge has been extensively studied [21–35]. However, conclusions based on those measurements are still ambiguous, and the physical picture of the process is obscure. The explanation of the breakdown physics based solely on the assumption of gas rarefaction with an increase in E/N, where E is the electric field, and N is the density of molecules at the atmospheric pressure [26], cannot fully describe the discharge evolution: appearance of fast and slow discharge modes [34] and the breakdown potential reduction. Moreover, these phenomena strongly depend on the geometric relation between the filament and the electrode.

The dynamics of LFP, before the breakdown, is also surely important to understand filament physics. Besides, LFP may find various applications as a point source of radiation in atmosphere: a source that is very sensitive to atmospheric conditions including atmospheric electric field. An interesting phenomenon has been found in pioneering experiment [37] on the terahertz radiation of LFP: the intensity of the radiation is very sensitive to the external field strength. The UV radiation of LFP has been also found very sensitive to external field strength [38–43]: it increases nonlinearly with the applied voltage. The field dependency of UV emission may become a basis for the remote field measurements in the atmosphere. However, there are various effects which can also result in the LFP emission such as the secondary emission, strong corona, runaway electrons, and so on and, therefore, can change the emission dependency on the field strength. The LFP, itself, may also affect the field distribution in the vicinity of measurements. To make a practical tool, we have to prove the conformity between the emission signal and the external field strength and the ability to maintain it. Detailed studies of LFP behavior in the external fields of different configurations are necessary to understand whether such measurement can be calibrated or can provide only the relative field measurements.

Interest in the effect of electron runaway in the atmosphere has been growing in the last decade, mostly due to the strong x rays observed by aircraft, satellites and ground detectors associated with thunderstorms [45–48]. The observation of hard x rays and γ-rays in conventional high-voltage discharges in the laboratory [49, 50] has also been reported. However, so far, the physics of the formation of runaway electrons in air and their acceleration is unclear.

LFP can be an excellent tool to investigate discharge physics including the electron runaway, because it can produce space charges instantaneously to control the initiation of atmospheric ionization precisely.

In this paper, we overview the kinetics and dynamics of the LFP in external electric fields of various configurations and its applications, such as the control of high-voltage discharges, including electron runaway, and the dynamics of UV emission from LFP for the applications of remote field measurement.

II. FILAMENT PLASMA INDUCED BY HIGH-INTENSITY FEMTOSECOND LASER PULSES AND ITS DYNAMICS IN STRONG EXTERNAL ELECTRIC FIELDS

LFP is produced in air by femtosecond laser pulses via the laser field ionization (multiphoton and/or tunnel ionization) [51]. A fs laser pulse undergoes the Kerr self-focusing in air [2, 7]; its intensity increases until an LFP is produced. Diffraction of the laser pulse in the plasma prevents any further self-focusing. The parameters of LFP such as the electron density and temperature strongly depend on the energy of laser pulses and focusing conditions. The electron density in LFP is about 10^{16}–10^{18} cm^{-3} (see Ref. [1, 2, 12, 18]), and the electron temperature is low; it is estimated to be ~ 0.5 eV [18]. A comprehensive analysis of the laser-filament dynamics in air can be found in Refs. [14]. Recently, the emission of laser filaments at several kilometer altitudes has been detected [6], ionization channels have been also observed over a distance reaching 400 m [10]. In addition, Kasparian *et al.* observed an increase of the number of cloud-cloud discharges using laser filaments, which shows the presence of plasma at several kilometer altitude [35]. These results suggest that the distant application of LFP, such as remote measurements of electric field and laser triggered lightning, is possible.

Figure 1 shows an image of plasma generated by a laser beam, when the beam was focused by a spherical mirror with a focal length of 20 m. In the inset of Fig. 1, multiple filaments are observed as bright lines [52]. Typical transverse profiles of filaments, produced when the laser beam was focused by a spherical mirror with 10 m focal length, in air without an external field are given in Fig. 2 (a)–(c) [34]. Multiple filamentation with transversely non-uniform plasma is detected. The appearance of plasma due to the Kerr self-focusing is clearly seen after the pulse passes over 7 m from the spherical mirror. The plasma filament is not uniform in the direction of laser pulse propagation. Fig. 2 (d) shows the calculated electron density distribution along a single filament [34]; it has many peaks in this direction reflecting the process of laser pulse focusing and defocusing.

The LFP is not a conventional discharge plasma or laser-breakdown plasma. Even in a strong electric field, LFP is cold and the dissociation recombination reduces the LFP electron density quickly: $N_e = N_{e0}/[1 + \beta N_{e0} t]$, where $\beta \sim 2 \times 10^{-7}$ cm^3/s [20, 53] and N_{e0} is the initial electron density in the filament. At $t \leq (\beta N_{e0})^{-1} \sim$ (5 – 500 ps), the LFP is dense, the Debye radius is smaller than a plasma size; electrons do not attach to oxygen molecules. [In this regime, the LFP acquires and maintains a minimal potential in its vicinity.] For $t > (\beta N_{e0})^{-1}$, the electron density loses the information on the initial value. Although the dissociation recombination reduces the plasma charge shortly (~ 100 ns) [20], the electron density $N_e = 5 \times 10^{14}$ cm^{-3}, at which the electron attachment to molecules

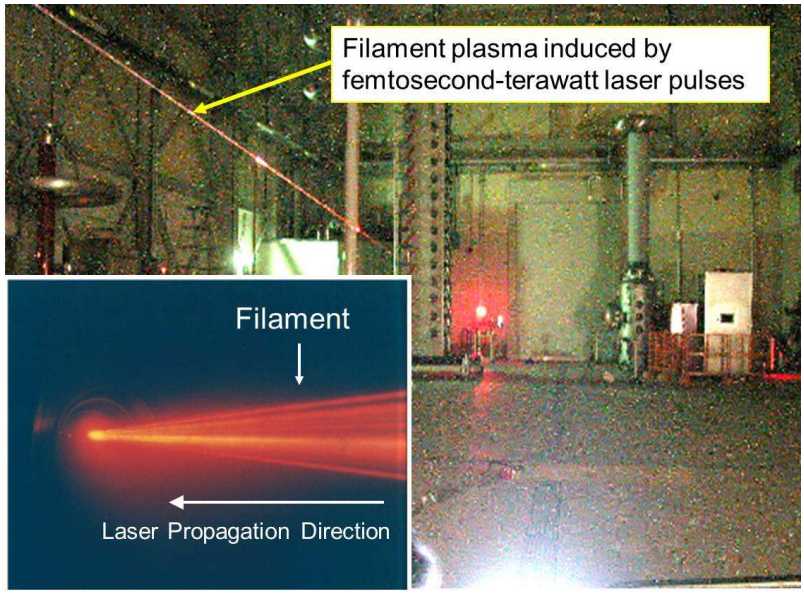

FIG. 1: (Color online) Multiple filamentation produced by ultrashort laser pulses.

becomes dominant and the density of negative ions rapidly grows, is much higher than that of electron avalanches preceding a natural breakdown. In this range, discharge between the electrode and LFP, electrons avalanches and streamers heat up plasma and change filament plasma dynamics. The filament can maintain an electrode potential necessary for the breakdown development and can become a leader, which leads to the filament-triggered breakdown.

III. NUMERICAL MODELING OF DYNAMICS OF LASER FILAMENT PLASMA IN EXTERNAL ELECTRIC FIELD

Dynamics of laser filament plasma in an external, near corona threshold field was studied by 2D3V particle-in-cell (PIC) simulation including elastic collisions $e - M$, $e - e$ (M means molecules) and the kinetic approach following [54] with variable particle weights. The electron-electron collisions were included because they are dominant if the electron density exceeds 10^{14} cm^{-3}. Only five sorts of particles have been included: electrons, negative oxygen ions, positive oxygen and nitrogen ions, and meta-stable nitrogen molecules. Assuming the rapid association, $A + A + B- > A_2 + B$ where B is an O_2 or N_2 molecule, we attributed the ions to O_2^- and $O_2^+ = X^+$ and $N_2^+ = Y^+$. The weight of particles was calculated in the kinetic cells according to the balance equation [20]. For the electron part

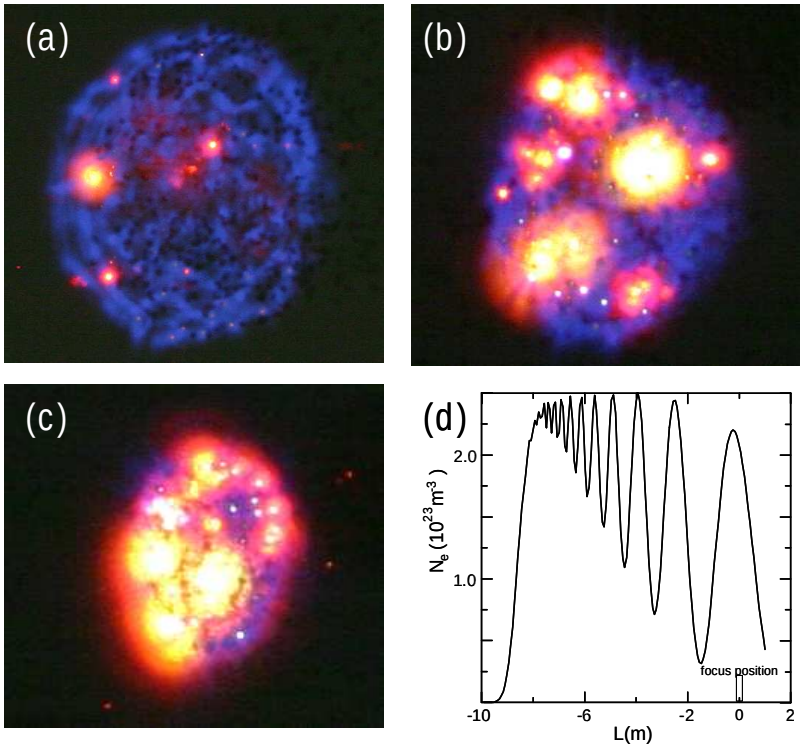

FIG. 2: (Color online) Transverse filament images after (a) 6.5 m, (b) 7.9 m, and (c) 9.2 m propagation from the spherical mirror; (d) calculated longitudinal distribution of electron density for a laser pulse with a peak power $P = 100P_{cr}$ and 70 fs pulse width in air. [34]

it is,

$$\frac{dN_e}{dt} = \left[\alpha^X_{ion}(E/N)N_X + \alpha^Y_{ion}(E/N)N_Y\right] N_e + \pi_P N^2_{Y^*} - \left[\beta^X_{DR}N_{X^+} + \beta^Y_{DR}N_{Y^+}\right] N_e - \nu_{Atach}N_X N_e$$

where α^M_{ion} is the ionization rate of M molecule calculated with the sampling electron distribution in PIC, π_P is the rate of Penning reaction; β^M_{DR} is the dissociative recombination rate for M ions, and ν_{Atach} is the electron attachment rate. In the ion part, the ion-ion recombination of positive and negative ions [20] was included as well. The UV emission was calculated using the simplified 2 level approximation with the sampling electron distribution from the PIC. In the present calculation the Penning and radiation effects were small.

We used Buneman scheme and calculated the electric field using pair of Maxwell equations:

$$\partial\vec{E}/\partial(ct) = \vec{\nabla}\times\vec{B} - 4\pi\vec{j}$$
$$\partial\vec{B}/\partial(ct) = -\vec{\nabla}\times\vec{E}$$

with the initial conditions found from a solution of Poison equation

$$d^2\phi/dx^2 = 0; -\nabla_\perp\phi|_{boundary} = \vec{E}$$

The simulation geometry is shown in Fig. 3. Results of the simulation for three different filament plasma shapes are shown in Fig. 4, 5, and 6.

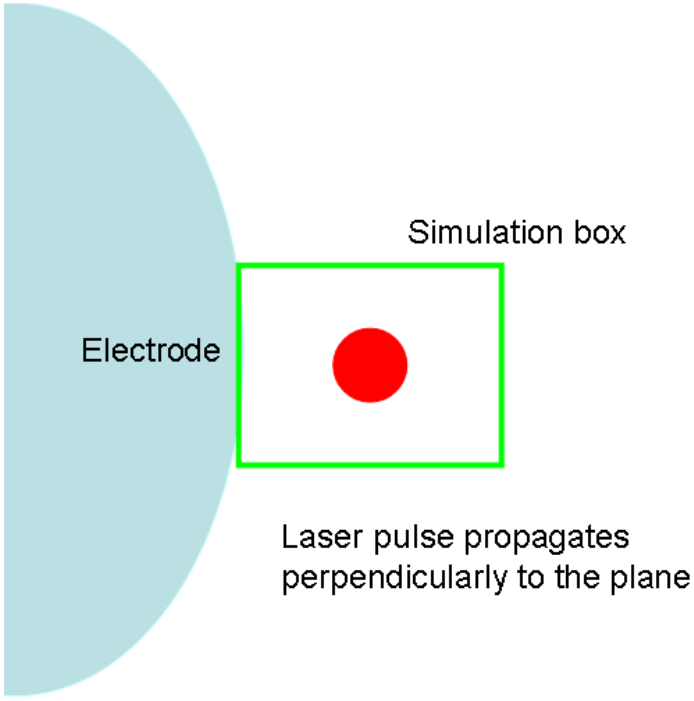

FIG. 3: (Color online) Simulation area. The initial field is directed from the left to the right.

One can see that electric field strength in the case of needle filament plasma approaches to the critical field for the electron runaway [39]. As seen in Fig. 7, the ionization wave are formed in the both sides of the filament plasma and are typical both for the negative and positive streamers.

IV. TRIGGERING AND GUIDING HIGH-VOLTAGE DISCHARGES (DISCHARGE CONTROL)

In 1995, Zhao *et al.* [21] reported the laser triggered discharges using laser pulses with the pulse length of 200 fs. After that, Pepin *et al.* [25] succeeded in triggering and guiding large-scale leader discharges over distances of 3 m with a megavolt impulse using sub-joule ultrashort laser pulses. From 2002, Teramobile group has reported on long gap laser-triggered discharges using the filament plasma produced by mobile terawatt laser system [27]. They have demonstrated the laser triggered discharges in 4.5 m gap length

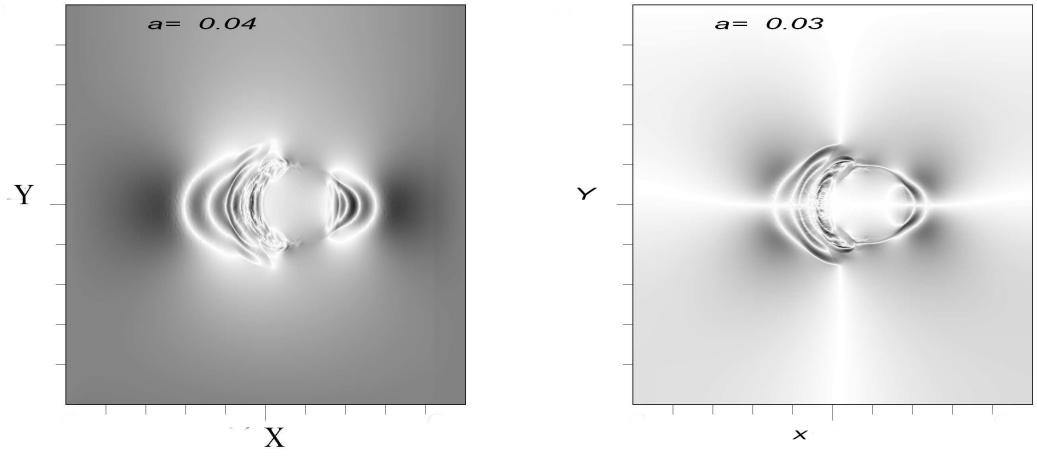

(a) (b)

FIG. 4: The x-(a) and y-(b) components of electric field near the laser filament plasma of cylindrical shape. Diameter of the filament is 0.5 mm. $E_x(0) = 29$ kV/cm, a is the normalized field strength; $a(0) = 0.02$. [41]

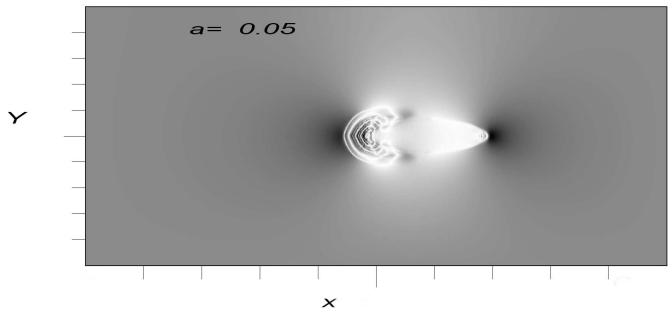

FIG. 5: The x-component of electric field near the laser filament plasma of elliptical shape. The filament is 0.3×1 mm^2.

with 2.2 MV negative impulse voltage using slightly focused femtosecond terawatt laser pulses [55]. They also tried to initiate the laser triggered natural lightning, and, finally, observed the sine of laser-triggered cloud-cloud lightning [35]. Recently, triggering and guiding of AC high voltage discharges has been performed using Tesla coil, which is promising for

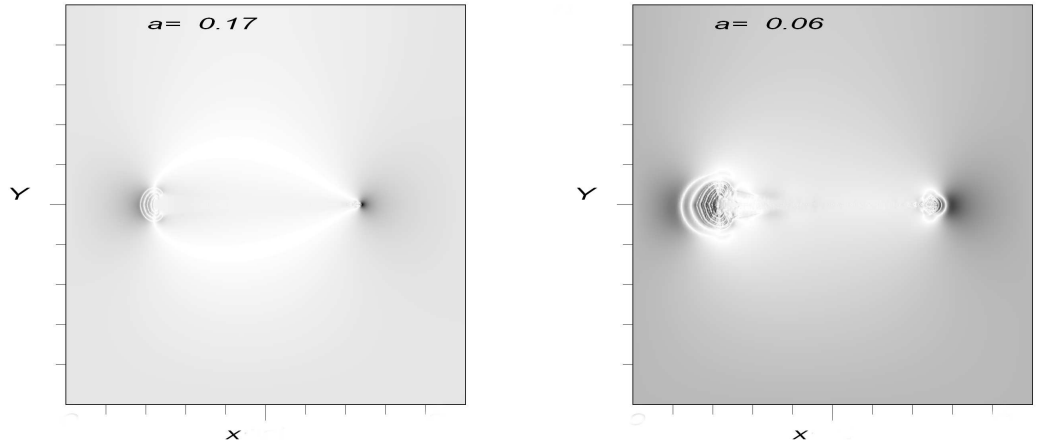

FIG. 6: Dynamics of x-component of electric field near the laser filament plasma of needle shape. The filament is 0.1×1 mm^2.

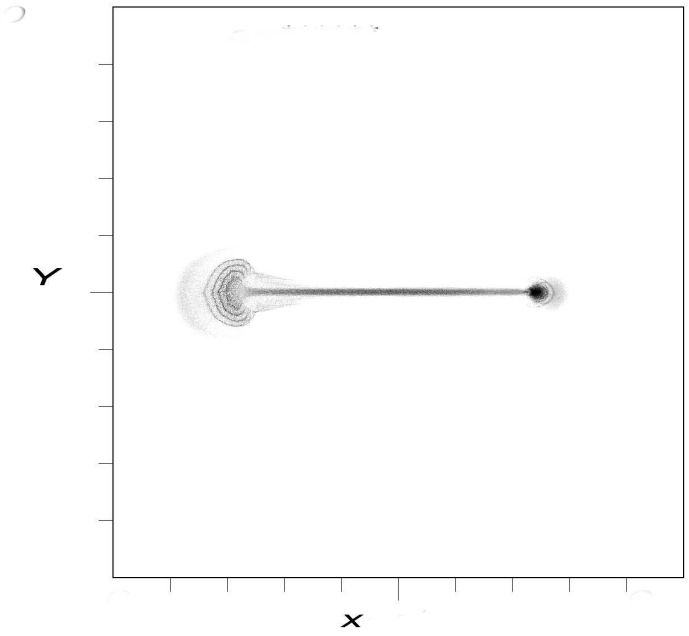

FIG. 7: Electron density in the laser filament plasma of needle shape. The filament is 0.1×1 mm^2.

a compact high voltage source [56–58].

However, in the case of natural lightning, the electric field may increase slowly before stroke. This phenomenon resembles the dc-discharge. An upward leader induced by lightning often has the positive polarity. Therefore, the study of the triggering and guiding of dc-high-voltage discharges is important for the operation with the natural lightning.

We have reported on temporally and spatially resolved measurements of dynamics of laser filaments in a strong electric field produced by positive dc voltages up to 0.44 MV for a gap length of up to 1 m, and their effects on the breakdown [34]. A typical time-integrated UV emission of the filament plasma in the external field without the breakdown, and that with the breakdown along the filament, are shown in Fig. 8. Bright emission between the grounded electrode and filaments, which may show the electron flow, is clearly seen. Other effects of plasma non-uniformity are illustrated in Fig. 9 by time-integrated discharge images. It is clearly seen in Fig. 9 (a) that the discharge stroke hops in the transverse direction. This indicates that the discharges occur via hopping between filaments having maximum electron density [32], which is also a sign of plasma non-uniformity as shown in Fig. 2. Figure 9 (b) shows a time-integrated plasma emission taken using the UV lens. Traces of electron avalanches can be seen from a location far from the electrode in both directions toward the electrode and toward the coronae.

Figure 10 shows dependency of the breakdown voltage versus the breakdown delay time for various distances between the laser filament and the 50-mm-spherical grounded electrode at a gap length of 0.6 m. Two completely different groups of discharges are observed. In Fig. 10, the first, which is called fast mode discharge, occurs after several microseconds from the laser shot with frequently the considerable breakdown voltage reduction. The second, called the slow mode discharge, occurs after more than several hundred microseconds from the laser shot without an essential breakdown voltage reduction. In the fast mode discharge, the maximal breakdown voltage reduction is ~ 40 % from the natural breakdown voltage, whereas it is only 4–10 % in the slow mode discharge. To investigate the fast and slow mode discharges, we have performed time-resolved measurements of plasma current and light emission.

Fig. 11 (a) shows a typical electrical current waveform along with the photodiode signal of laser shot. It demonstrates the typical behavior of the streamer breakdown. The first current signal shows that the primary streamer, installed near the high-voltage electrode immediately after the laser shot, reaches the grounded electrode after 3 μs from the laser shot. The estimated streamer speed is about 10^5 m/s, which agrees well with the results of previous streamer measurements [20, 59, 60]. The rise of the main current pulse, which is attributed to the ionizing waves and the secondary streamer [59, 60], is seen after about 100 ns from the first current signal. Therefore, one may estimate the speed for the potential wave [20, 59] as close to 10^7 m/s.

Fig. 11 (b) shows a temporally and spatially resolved image of plasma radiation in the fast mode discharge without an essential breakdown voltage reduction. Localized emission, corresponding to the first current and being shown in Fig. 11 (a), is observed 200-300 ns before the breakdown near the grounded electrode (position A). After several tens of nanoseconds, strong local emission is also observed at 150 mm from the high-voltage

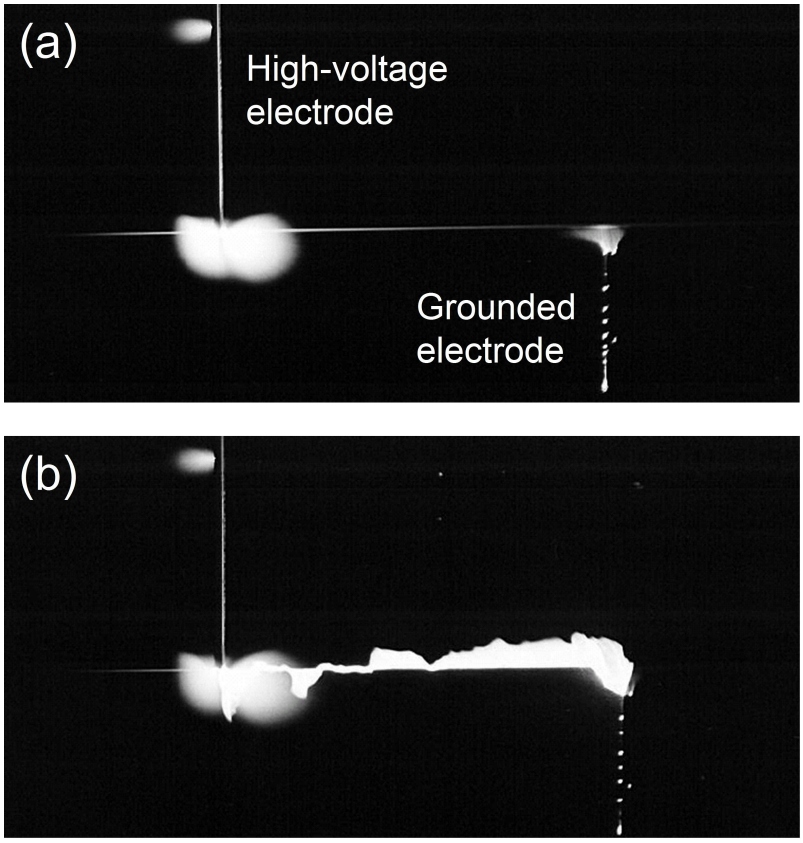

FIG. 8: (a) Filament emission without discharge at 0.28 MV voltage, and (b) discharge along the filament at 0.30 MV voltage with a gap length of 0.6 m. [34]

electrode (position B). One can see that ionizing waves correlating with bright plasma emission appear and exist in the gap between position A and B. The estimated speed of the ionizing wave is about 10^7 m/s, which agrees well with the measurement result in Ref. [60]. Appearance of a strong emission in position B can be attributed to the leader head.

The ionizing waves repeatedly appear in the plasma channel with strong field inducing the Ohmic heating of the plasma channel if the electron attachment rate in air plasma increases with the electric field [59, 60]. This is possible if the average field exceeds the critical value for air, $< E/N > \sim (2/3) \times 10^{-20}$ Vm^2. The fast mode discharge appears if the first streamer induces enough electrons from the grounded electrode to start the secondary streamer [20, 59, 60]. Moreover, the fast mode discharge with a considerable breakdown voltage reduction can occur only along with an artificial leader generated by the filament. The reduction of breakdown voltage is determined by the leader length in this case. Occurrence of the leader only in the fast mode discharge and the strong fluctuation of the breakdown voltage shown in Fig. 10 reflect a short lifetime of the filament-induced leader.

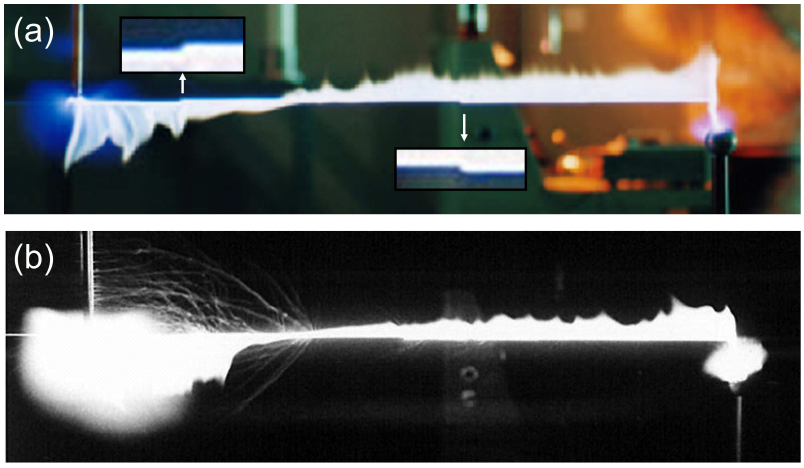

FIG. 9: (Color online) Photographs of laser-induced discharges in a 1-m-long gap taken using (a) a normal lens at a voltage of 0.4 MV and (b) a UV lens and a filter (blocking: 400–800 nm) at a voltage of 0.44 MV. No discharge is occurred up to 0.5 MV without laser filaments. [34]

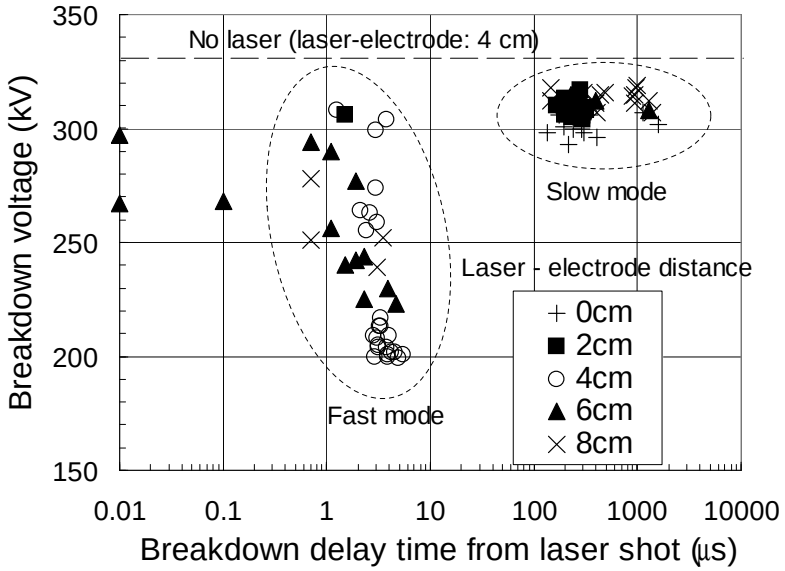

FIG. 10: Dependency of the breakdown voltage on the breakdown delay time at various distances between laser beams and the 50-mm-diameter spherical grounded electrode at a gap length of 0.6 m. [34]

We attribute the slow mode discharge to a weaker emission of electrons from the grounded electrode, lower than that necessary for developing of the secondary streamer. For initiating a new primary streamer, the negative and positive ions should be distant by the external field at $\delta L \sim 1$ cm [20, 60]. With an ion mobility $\mu \sim 2 \times 10^{-4}$ m^2/Vs in

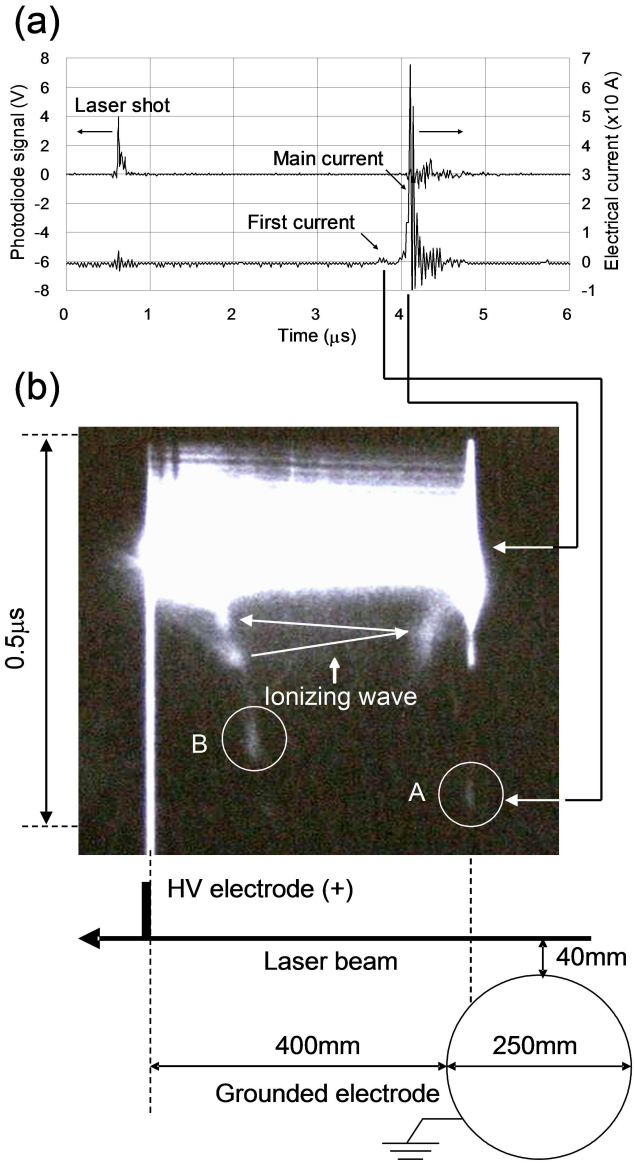

FIG. 11: (a) Electrical current and photodiode signal of laser shot and (b) image converter camera image of a fast mode discharge along with the experimental setup with an applied voltage of 0.275 MV on a 0.4 m-length gap using the 250-mm-diameter spherical grounded electrode. The self-breakdown voltage is 0.28-0.285 MV. [34]

air, it gives a time $T_{slow} \sim \delta L/\mu E \sim 0.5$ ms for $E = 0.5$ MV/m, which is typical for the experimental conditions.

V. LFP EFFECTS ON CORONA DISCHARGES

In this chapter, we discuss the dynamics of UV emission from LFP with a high spatial and temporal resolution when the electric field strength near the electrode surface only slightly exceeds the corona discharge threshold ~ 30 kV/cm [39].

V-1. Experimental setup

The scheme of the experimental setup is shown in Fig. 12. Ti:Sapphire laser pulses ($\lambda = 800$ nm, $\tau = 50$ fs, energy $= 84$ mJ) were focused by a concave mirror of 10 m focal length. A negative or positive high voltage was applied on a spherical high voltage electrode (HVE) with 250 mm diameter placed at the distance of 10.4 m from the focusing mirror. A high voltage was varied between 0 kV and + 400 kV or – 400 kV. The optical axis of the laser pulse was set at 5 mm, 6.8 mm or 28 mm from the HVE. The fluorescence of LFP was collected by a telescope located 20 m far from the HVE. The fluorescence was detected by a spectrometer and by an ICCD camera. UV images of LFP were taken by another ICCD camera with UV lens and a filter placed at 4 m from HVE perpendicularly to the laser axis. A still camera with the UV lens and the filter was set with a film slightly beside the UV-ICCD camera.

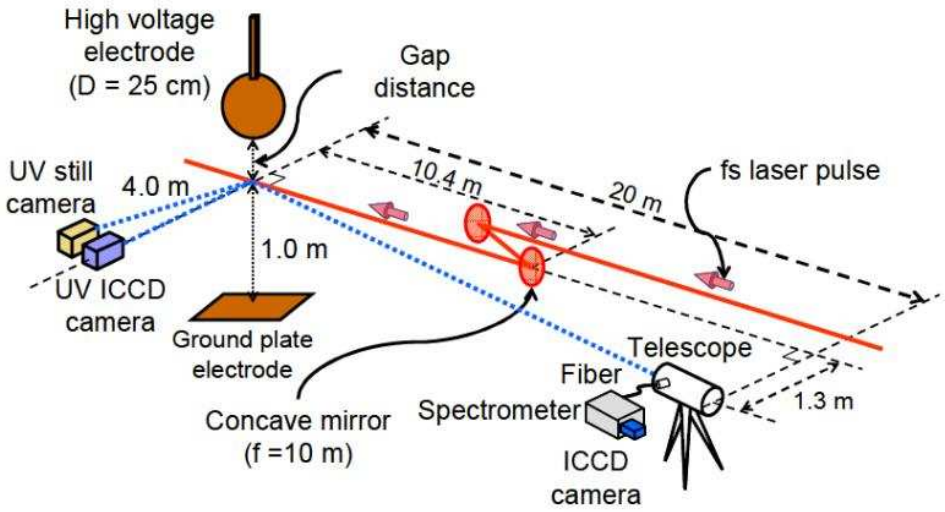

FIG. 12: (Color online) Experimental setup for investigation of corona bursts. [39]

V-2. Experimental results

V-2-1. Negative polarity

Images illustrating the voltage dependence and the temporal behavior of the negative corona at different voltages are shown in Figs. 13 and 14 in the presence of the LFP

positioned at 5 mm or 6.8 mm from the HVE surface. The corona discharges are caused by the LFP already at $U = -200$ kV, and become stronger at the higher applied voltages up to $U \sim -400$ kV. Visibly, there was no corona discharge in the absence of the LFP at any voltage applied up to $U \sim -400$ kV. The LFP induced corona discharges exhibit a complicated dynamics and spatial structure.

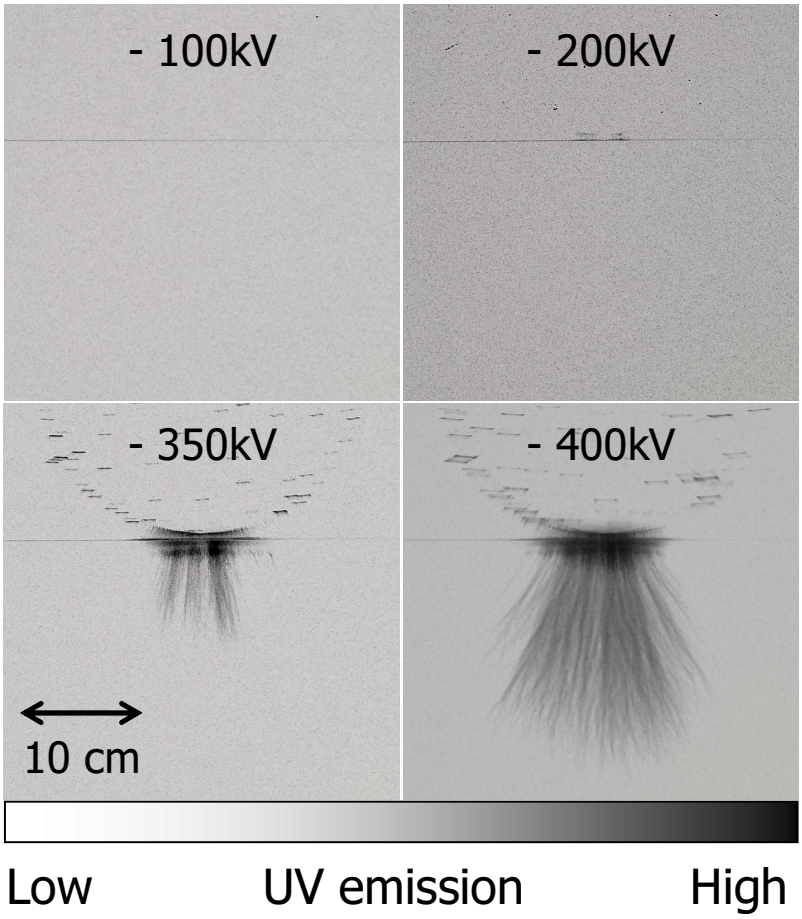

FIG. 13: UV-still images of the negative corona induced by LFP positioned at 5 mm from the HVE surface at several applied voltages from −100 kV to −400 kV. [39]

When the LFP appears below the HVE, the filament electrons move outwards. The recombination of the LFP is so rapid that the ions from the plasma cannot reach the electrode to cause the secondary emission: ion mobility is about $\mu = 2.1$ cm^2/V/s [20] and the velocity is about 10^5 cm/s at $E \sim 50$ kV/cm and is surely too low for that: the process ceases in 1 μs as shown below. However, the LFP may affect the corona discharge via the UV flash which appears just after the creation of LFP and the consequent electron emission from the electrode. The latter assists the discharge developing between the LFP and the electrode.

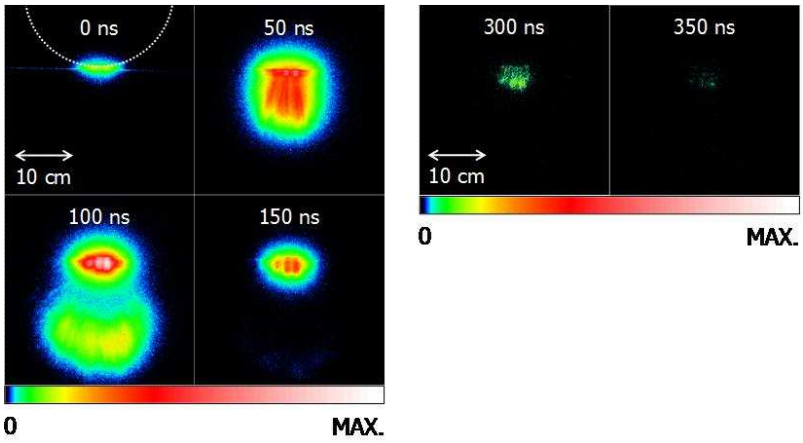

FIG. 14: (Color online) UV-ICCD images of the negative corona induced by LFP positioned at 6.8 mm from the HVE surface with the applied voltage of −400 kV at several gate delay times of the ICCD camera from 0 ns to 350 ns. The maximal values of color bar are 25,000 for 0/150 ns and 2,500 for 300/350 ns. The gate width and gain of the ICCD camera are 50 ns and 250, respectively. [39]

Assuming that the electrode electric field does not change much along the LFP in the beginning, one can get the filament filed as ~ 60 kV/cm in the experimental conditions using the conventional estimation: $E_f = -\Lambda U_0 \cdot R_0/R_f^2$, where U_0 is the electrode potential, R_f is the filament position from the center of the electrode, Λ is the geometrical field gain: for a cylindrical filament $\Lambda = 2$. In the absence of inelastic collisions, the LFP electrons would have acquired the average energy, $\bar{\varepsilon} \sim \sqrt{M/3m}(eEl)$, with l the electron free-path and M the ion mass. For the field in the experiment this value is about 1 keV. Therefore under the experimental conditions, an LFP electron is accelerated and loses its energy for the ionization and excitation till it forms a negative ion in the reaction: $O_2 + e \rightarrow O^- + O$ ($\varepsilon_{\max} \sim 8$ eV). Then, the strong radiation ceases. The intensity of UV flashes depends on the field strength [38–43] and plays an important role in the LFP dynamics.

The UV radiation from the LFP may initiate the electron emission from the electrode. This results in the rapid discharge between the LFP, becoming a virtual anode, and the cathode. This can be seen in Figs. 13 and 14. If the breakdown appears swiftly, the electron density in LFP is high and the LFP acquires the cathode potential because its capacity is much lower than that of the cathode. As a result, the field at the LFP surface drastically changes: $E_f = -U_0/D$. Since $D \sim 200$ μm the field may become very high, ~ 10 MV/cm. Apparently the real field is smaller because the electron density in LFP decreased so rapidly that the LFP cannot maintain the whole electrode potential. Nevertheless such a field is strong enough to provoke the streamer developing outward from the LFP.

Dynamics of the corona discharge in the case of $U_0 = -400$ kV is given in Fig. 14. One can see the two distinct regions. Figure 15 shows the temporal and spatial evolution of UV emission at the axis perpendicular to the laser filament through the center of the HVE obtained from the results shown in Fig. 14. As shown in Fig. 15, the UV emission

spreads over 200 mm far from the electrode for about 100 ns. On the other hand, the emission at the filament position continuously increased in the first 100 ns. The velocity of the UV emission front was estimated to be 0.6 % of the speed of light. As seen from Figs. 14 and 15, the strong streamer radiation at a distance quite far from the electrode lasted for $\sim$ 150 ns, and the post-plasma recombination radiation emitted for $\sim$ 0.5 μs. Such a long emission can be produced by a hot plasma; in our case the best fitting gives $T_e \sim 10$ eV and $N_e \sim 10^{15}$ cm^{-3} (from local kinetic simulations [20]). This velocity agrees well with the velocity of the streamers [19]. The two distinguished regions may just reflect (i) the radiation of the streamer heads, far from the electrode, and (ii) the radiation of recombining LFP.

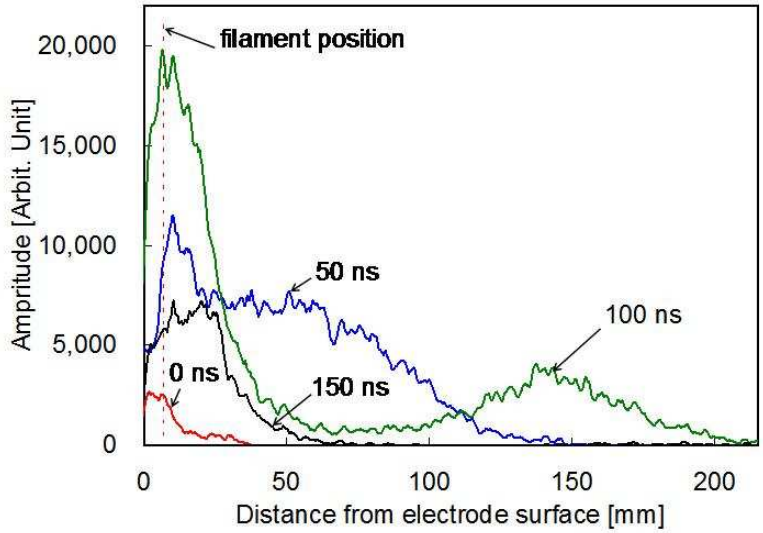

FIG. 15: (Color online) Temporal and spatial evolution of UV emission in the cross section perpendicular to the laser filament obtained from the UV-ICCD images shown in Fig. 14. The cross section is vertically through the point on filament that is the closest to the electrode surface. [39]

The voltage dependence and temporal evolution of the UV spectra in the vicinity of LFP detected by the telescope is presented in Fig. 16 for the 313.6 nm, 315.9 nm, and 337.1 nm nitrogen lines ($N_2 : C^3\Pi_u \rightarrow N_2 : B^3\Pi_g$). The temporal evolution of the peak signal height of N_2 fluorescence well corresponds to that of the UV emission in the vicinity of LFP as seen in Fig. 15. One can find the strong dependence of the UV spectra on the external voltage. These UV spectra can be used for the electric field diagnosis.

V-2-2. Positive polarity

We have also tested the positive corona as shown in Fig. 17 and 18 upon positioning the LFP at 5 mm from the HVE surface. Again in the absence of the LFP, we observe no corona discharge. However, the LFP drastically changes the corona dynamics.

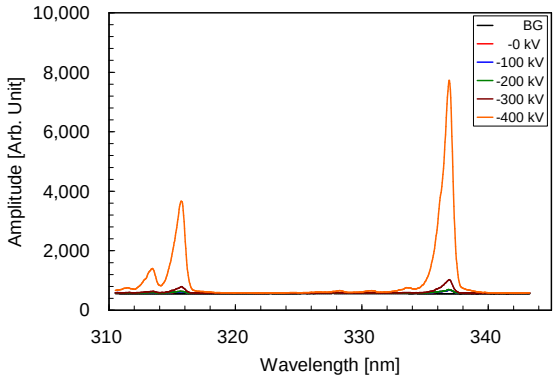

(a)

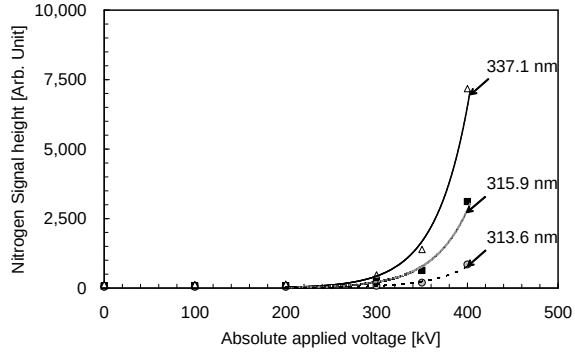

(b)

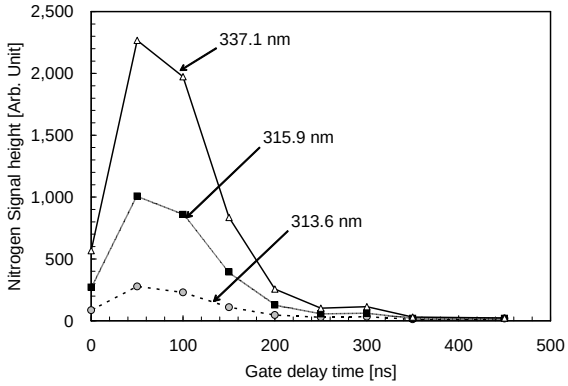

(c)

FIG. 16: (Color online) Fluorescence spectra of N_2 molecules and peak signal height of the N_2 fluorescence for the wavelengths of 313.6 nm, 315.9 nm, and 337.1 nm in the vicinity of the HVE and filament when the optical axis of the laser beam is set at 5 mm from the HVE surface for the negative polarity. (a) Fluorescence spectra of N_2 molecules at several applied voltages and background spectra (shown as BG) taken at a voltage of -400 kV without the LFP, (b) peak signal height of the N_2 fluorescence over background spectra as a function of applied voltage, (c) peak signal height of the N_2 fluorescence over background spectra as a function of the gate delay time of the ICCD camera with the applied voltage of -400 kV. The gate width and delay time of the ICCD camera for the experiments shown in (a) and (b) are 500 ns and 0 s, respectively. The gate width of the ICCD camera for the experiments shown in (c) is 50 ns. [39]

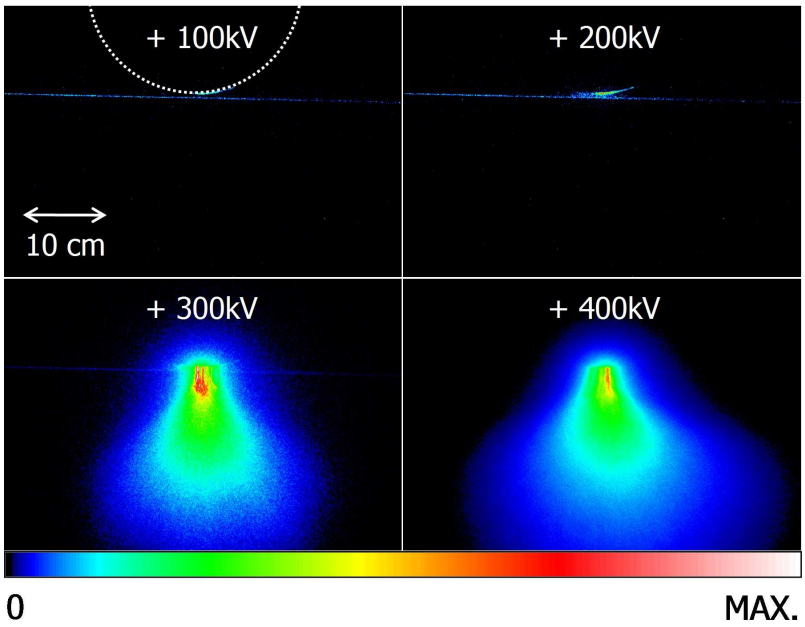

FIG. 17: (Color online) UV-ICCD images of the positive corona induced by LFP positioned at 5 mm from the HVE surface at several applied voltages from 100 kV to 400 kV. The gate width and delay time of the ICCD camera are 500 μs and 0 s, respectively. The gain of the ICCD camera is 250 for 100/300 kV and 50 for 400 kV. The maximal values of color bar are 3,000 for 100 kV/200 kV and 30,000 for 300 kV/400 kV. [39]

In the figures, one can see a scenario that is expectedly different from the scenario for the negative streamer. In this case one can expect a stronger effect of the LFP because the electrons from the plasma could reach the electrode: the necessary time is about 20 ns since electron mean velocity in air at the field strength $E \sim 30$ kV/cm is not high, about 2×10^7 cm/s [20]. However, the electron evacuation must be rapidly ceased when $U_0 R_0/R^2 \sim U_f/D$ where R is a distance between the center of HVE and the filament, and U_f is the LFP potential; this process results in the strong initial UV emission from LFP. In the case of the positive polarity, the UV emission cannot provoke a discharge between the LFP and electrode; the UV emission may only pre-ionize air to stimulate the positive streamers as seen in Fig. 18 where the snapshots of the positive corona are presented.

VI. RUNAWAY ELECTRONS

In this chapter, we present and discuss the effects of the electron runaway in positive high-voltage-impulse discharges studied via detecting hard x ray spectra [61]. LFP is used to localize the source of runaway electrons. We will not consider the relativistic avalanches provoked by the cosmic rays in the atmosphere [62].

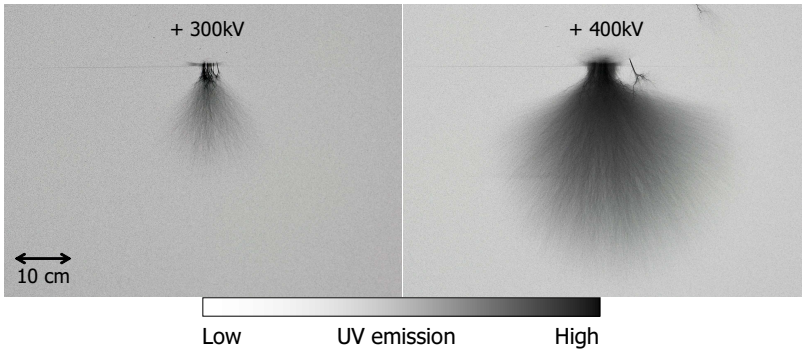

FIG. 18: UV-still images of the positive corona induced by LFP positioned at 5 mm from the HVE surface at applied voltages of 300 kV and 400 kV. [39]

The effect of runaway electrons in gas discharges occurs in rather strong electric fields. For an electron to run away, it has to acquire kinetic energy from a field greater than the energy it lost by ionization, excitation, and dissociation of air molecules. The threshold field strength, E_{RW}, for $\sim$ 1–10 eV energy electrons in the normal-pressure air is about $E_{RW} \sim 320$ kV/cm. However, the maximum field strength in the atmosphere is approximately $\sim$ 29 kV/cm [20]; the typical field strength in a thunderstorm is $\sim$ 1 kV/cm [63]. There is another way of allowing electrons to run away by increasing their free paths by reducing the air density, increasing their initial energy (cosmic rays), and/or by preheating the electrons. The joint effect of a strong electric field and preheated plasma likely results in the formation and acceleration of electrons in air at lower electric field strengths.

In our experiments, brass balls of 250 mm diameter were used as the high-voltage electrode (HVE) and the grounded electrode with a gap length of 0.45 m. Positive impulse voltage, which reached its maximum at ~ 0.6 μs, was applied on HVE. The charging voltage (CV) applied at the impulse generator was set at 650 or 750 kV. Ti:sapphire laser pulses with 70 fs duration and 90 mJ energy were focused by a concave mirror of 10 m focal length, placed at the distance of $\sim$ 10 m from the electrodes, and LFP was produced in the gap. Cylindrical detectors, each composed of a NaI (Tl) scintillator and a photomultiplier tube (PMT), were used for measuring x rays signals from the sparks. The detectors were placed at about 3 m from the electrodes perpendicularly to the laser axis.

As shown in Fig. 19, the breakdown plasma channel is strongly convoluted and a lot of streamers generating from HVE are observed without using LFP. On the other hand, when LFP was produced at 5 mm from the HVE, the breakdown plasma channel is rather straight, and there is less number of streamers generating from HVE. This is also confirmed by detector signals showing the dark current (a small current before the breakdown) presented in Fig. 20. The voltage just before an x-ray burst was about 550 kV, and the electric field strength near the grounded electrode, according to [64], was about 10 kV/cm. Therefore, streamers resulting in the dark current can propagate only from the HVE.

More than 50% of all the discharges without LFP were accompanied by x ray bursts.

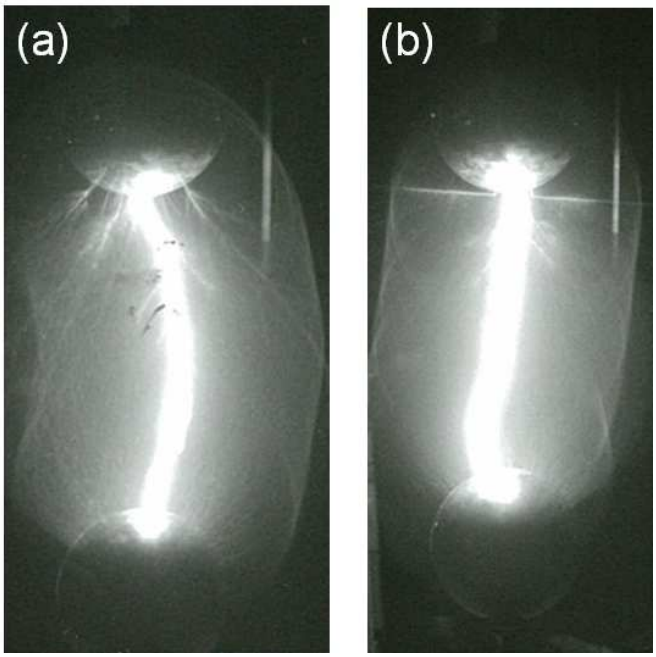

FIG. 19: Photographs of discharges (a) without and (b) with LFP with a CV of 650 kV taken using a UV lens and a filter (blocking: 400–800 nm). [61]

As shown in Fig. 20, the bursts, which should originate from the Bremsstrahlung radiation generated by runaway electrons in the positive electrode, always occur before the breakdown. The Bremsstrahlung radiation was always synchronized with the beginning of the dark current.

To evaluate the spectrum of x-rays, we used the absorption technique [49]: x-rays were detected with Pb or Al shields in front of the detector. The depletion of the signals with the attenuator thickness is shown in the inset of Fig. 21. The experimental data are fitted with the calculated results using a Monte Carlo-type code (Geant4) [65]. In the calculation, we assumed an x-ray energy distribution $\sim \exp(-\varepsilon_x/\varepsilon_{x0})$ with an exponential shape, where ε_x is the x-ray energy and ε_{x0} is a fitting parameter. The best fitting energy, ε_{x0}, lies in the range of 50–100 keV. The main graph of Fig. 21 shows calculated backward x ray spectra from a massive brass target irradiated by monoenergetic electron beams with different energies. Each spectrum has also been fitted by an exponent of $\sim \exp(-\varepsilon_x/\varepsilon_{x0})$. By comparing these values of ε_{x0} with that determined in the inset, one can see that the electron energy before interaction with the brass must be approximately 500–700 keV, which is close to the applied potential. These results suggest that the position of the source of runaway electrons should be near the surface of the negatively biased electrode.

The second evidence of the position of the runaway electron source was found with the use of the LFP before the breakdown as in [34, 39]. A laser pulse was shot at 0.5 ∓ 0.1 μs before voltage breakdown, which is the time that corresponds to the beginning of an

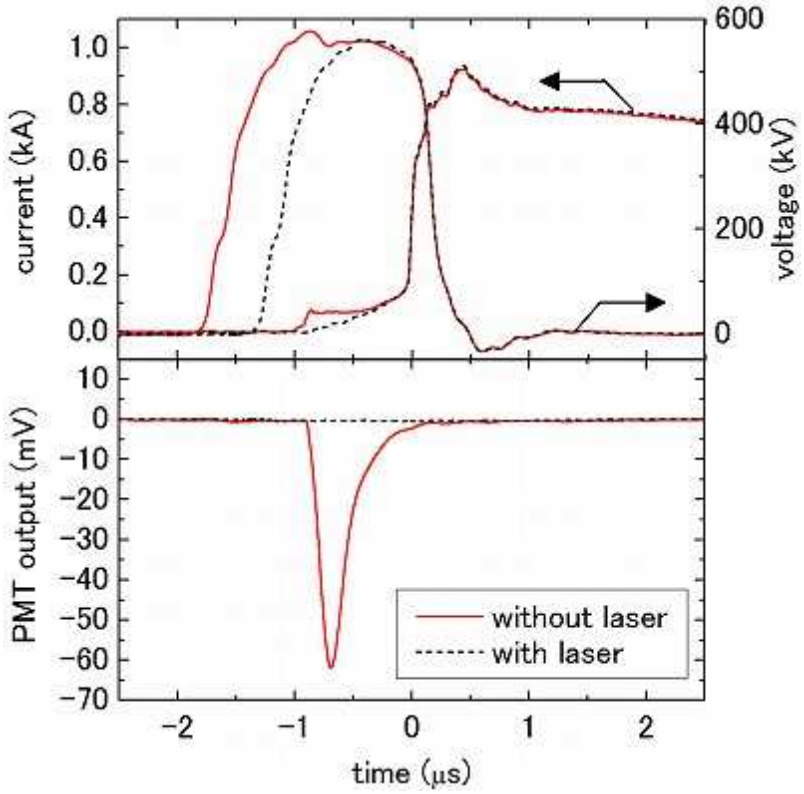

FIG. 20: (Color online) Typical waveforms of voltage, current, and PMT signal for discharges with and without LFP with a CV of 650 kV. [61]

x-ray burst in the case of discharges without the laser irradiation. The formation of LFP at 5 mm from the HVE stopped the x-ray burst in 100% of the cases, as shown in Fig. 20, whereas LFP 5 mm from the grounded electrode did not strongly affect the burst. As shown in Fig. 20, an essential dark current were not observed. On the other hand, LFP may affect the propagation of avalanches and streamers starting from the HVE, as discussed in [39], making the ionization wave [34, 60] weaker during the development of streamer discharge. We accept the following scenario for the runaway formation in the case of the positive polarity. A positive streamer propagates from the HVE to the grounded electrode and initiates a weak discharge (see also [19]) generating a plasma channel: the small current growth before the x-ray burst is always seen, as shown in Fig. 20. The plasma channel in the vicinity of the grounded electrode is heated, forming a short, pin-shape leader. Such a leader with a considerable number of ~ 1 keV electrons can be a source of the electron runaway resulting in the x-ray burst from the opposite electrode. When the LFP was ignited, the small dark current decreased and no pin-shape leader is formed, which also supports the above scenario.

2D PIC simulations, including elastic collisions and plasma kinetics, show the possi-

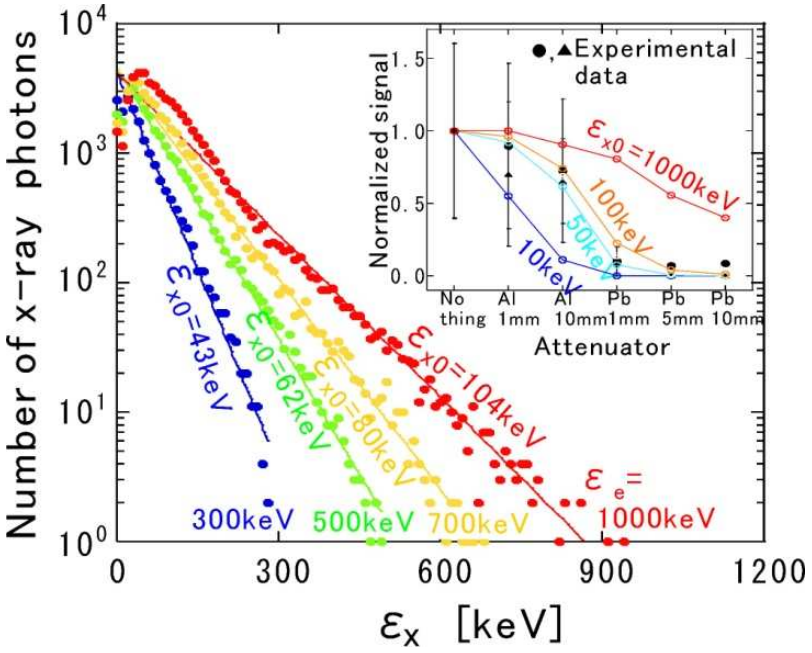

FIG. 21: (Color online) Calculated backward x-ray spectra from a brass target produced by electron beams with energies (ε_e) of 300 keV, 500 keV, 700 keV, and 1.0 MeV. The inset is the measured depletion of x-rays after attenuators with a CV of 750 kV, shown by solid circles (T_{room}: 15–18 centigrade, RH: 40 $\sim$ 56%, P_{atm}: 992–1000 hPa) and triangles (T_{room}: 14–15 centigrade, RH: 45-58%, P_{atm}: 985–993 hPa), and calculated curves for several fitting parameters of x-ray energy (ε_{x0}). [61]

bility of the formation of such a leader with electron runaway [61]. The runaway electrons are likely produced from preheated, $\sim$ 0.1-1-mm-size leaders with the electron density of $\sim 10^{14}$ cm^{-3}. The electrons can then be accelerated even by low-strength electric fields, $E < 30$ kV/cm.

VII. SUMMARY

The kinetics and dynamics of the LFP in external electric fields of various configurations are studied.

We have made time-resolved measurements of dynamics of plasma of laser-induced filaments in a strong external electric field for various field conditions and geometry. Two different discharge modes, fast and slow, have been found. Considerable reduction of breakdown voltage has been observed only in the fast mode. The non-uniform distribution of electron density along the filament strongly results in the discharge dynamics. The potential reduction appears when filaments induce the leader maintained by strong non-uniform field. We anticipate that the high predictability and well-determined position of the laser-filament

induced leader open a way of comprehensive study of leader-streamer physics.

We have performed the imaging and spectral measurement of UV from laser-filament plasma in an external field of different polarities produced by the spherical electrode. The field dependency of the UV emission has been shown to be useful at least for the relative field measurements (detection of field distribution). The discharges between the LFP and electrode plays the dominant role, and we have observed the long (tens of centimeters) positive and negative corona induced by the laser-filament plasma initiated by a femtosecond laser pulse in the vicinity of an isolated electrode without an initial corona. We have detected the different stages of the corona bursts: the initial UV flashes from the LFP; the UV flashes from discharge between the LFP as a virtual electrode and the real electrode; and UV from the streamer discharges. For the negative polarity, the UV emission peak observed at 15 cm far from the filament can be explained by the streamer developing at the velocity 0.6% of the speed of light.

The effects of electron runaway in positive high-voltage-impulse discharges have been investigated using the LFP to localize the source of runaway electrons. By measurement of the characteristics of x-ray bursts with and without LFP and via the numerical simulations, we have found that (i) sources of electron runaway are localized at the negative polarity electrodes even if this electrode is grounded. (ii) The runaway electrons in the discharges are likely produced from preheated, $\sim$ 0.1-1-mm-size leaders with the electron density of $\sim 10^{14}$ cm^{-3}, and formed on the surface of the electrode. The electrons can then be accelerated even by low-strength electric fields, $E < 30$ kV/cm. (iii) Those electrons acquire kinetic energies close to or probably even exceeding the potential difference between the electrodes resulting to produce the strong hard x rays.

The obtained results are very useful not only for understanding the filament physics but also for applications of filament such as discharge control, laser lightning rod, and remote measurement of electric field. In order to realize such applications, the control of filament is important. It was demonstrated that filaments can propagate well in adverse atmospheric conditions such as turbulence [66], foggy [67] or rainy [68] atmosphere partly due to the self-healing effect. However, precise control of the filament plasma position, which may depend on atmospheric conditions, has yet to be achieved. Thunder lightning can be occurred with much lower electric field ($\sim$ 1 kV/cm) than the theoretical value, but its mechanism is still unclear. The study of runaway electrons is surely useful for understanding the high energy physics in the atmosphere, which can lead to complete understanding of mechanisms of lightning. Recently, the runaway electron avalanche model, in which the runaway electron avalanche may pre-ionize air and initiate lightning, has been proposed to explain the phenomena. The necessary conformity of laboratory experiments and the field observation requires its further development.

In addition, huge amount of electricity is transported by using air as an electrical insulator. Since many electric power apparatuses use the air as an electrical insulator, discharge plasma in air is one of key issues in electric power industries. If we can simulate discharge characteristics, we can design and manage electric facilities far more efficiently. The LFP is the very attractive and flexible instrument for investigating plasma physics in air.

References

[1] A. Braun *et al.*, Opt. Lett. **20**, 73 (1995).
[2] B. La Fontaine *et al.*, Phys. Plasmas **6**, 1615 (1999).
[3] H. Yang *et al.*, Phys. Rev. E **66**, 016406 (2002).
[4] J. Yu *et al.*, Appl. Optics **42**, 7117 (2003).
[5] G. Méchain, A. Couairon, M. Franco, B. Prade, and A. Mysyrowicz, Phys. Rev. Lett. **93**, 035003 (2004).
[6] M. Rodriguez *et al.*, Phys. Rev. E **69**, 036607 (2004).
[7] S. Skupin *et al.*, Phys. Rev. E **70**, 046602 (2004); J. R. Penãno *et al.*, Phys. Plasmas **11**, 2865 (2004); S. Champeaux and L. Bergé, Phys. Rev. E **71**, 046604 (2005).
[8] S. L. Chin *et al.*, Can. J. Phys. **83**, 863 (2005).
[9] A. Ting, D. F. Gordon, E. Briscoe, J. R. Peñano, and P. Sprangle, Appl. Optics **44**, 1474 (2005); A. Ting *et al.*, Phys. Plasmas **12**, 056705 (2005).
[10] G. Méchain *et al.*, Opt. Comm. **247,** 171 (2005).
[11] R. Ackermann *et al.*, Opt. Lett. **31**, 86 (2006).
[12] F. Théberge, W. Liu, P. T. Simard, A. Becker, and S. L. Chin, Phys. Rev. E **74**, 036406 (2006).
[13] L. Bergé, S. Skupin, R. Nuter, J. Kasparian, and J.-P. Wolf, Rep. Prog. Phys. **70**, 1633 (2007).
[14] A. Couairona and A. Mysyrowicz, Phys. Rep. **441**, 47 (2007).
[15] Y. Chen *et al.*, Opt. Lett. **32**, 3477 (2007).
[16] S. Champeaux and L. Bergé, Phys. Rev. E **77**, 036406 (2008).
[17] Y. Ma, X. Lu, T.-t. Xi, Qi-h. Gong, and J. Zhang, Opt. Express **16**, 8332 (2008).
[18] J. Bernhardt *et al.*, Opt. Comm. **281**, 1268 (2008).
[19] L. B. Loeb and J. M. Meek, *The Mechanism of the Electric Spark* (Oxford University Press, Oxford, 1941).
[20] Y. P. Raizer, *Gas Discharge Physics* (Springer-Verlag, 1991).
[21] X. M. Zhao, J.-C. Diel, C. Y. Wang, and J. M. Elizondo, IEEE J. Quantum Electron. **31**, 599 (1995).
[22] L. Fontaine *et al.*, IEEE Trans. Plasma Sci. **27**, 688 (1999).
[23] B. L. Fontaine *et al.*, J. Appl. Phys. **88**, 610 (2000).
[24] D. Comtois *et al.*, Appl. Phys. Lett. **76**, 819 (2000).
[25] H. Peppin *et al.*, Phys. Plasmas **8**, 2532 (2001).
[26] S. Tzortzakis *et al.*, Phys. Rev. E **64**, 57401 (2001).
[27] M. Rodriguez *et al.*, Opt. Lett. **27**, 772 (2002).
[28] D. F. Gordon *et al.*, Phys. Plasmas **10**, 4530 (2003).
[29] D. Comtois *et al.*, IEEE Trans. Plasma Sci. **31**, 377 (2003).
[30] J. Kasparian *et al.*, Science **301**, 61 (2003).
[31] T. Fujii *et al.*, IEEJ Trans. FM **125**, 765 (2005) (in Japanese).
[32] N. Goto *et al.*, IEEJ Trans. FM **125**, 1059 (2005) (in Japanese).
[33] G. Méjean *et al.*, Appl. Phys. Lett. **88**, 021101 (2006).
[34] T. Fujii *et al.*, Phys. Plasmas **15**, 013107 (2008).
[35] J. Kasparian *et al.*, Opt. Express **16**, 5757 (2008).
[36] S. Tzortzakis *et al.*, Opt. Lett. **27**, 1944 (2002).
[37] A. Houard, Y. Liu, B. Prade, V. T. Tikhonchuk, and A. Mysyrowicz, Phys. Rev. Lett. **100**, 255006 (2008).
[38] K. Sugiyama *et al.*, Opt. Lett. **34**, 2964 (2009).
[39] K. Sugiyama *et al.*, Phys. Plasmas **17**, 043108 (2010).
[40] T. Fujii *et al.*, CRIEPI report H09020 (2010).

[41] T. Fujii *et al.*, J. Plasma Fusion Res. **86**, 669 (2010) (in Japanese).
[42] T. Fujii, *in Industrial Applications of Laser Remote Sensing*, eds. T. Fukuchi and T. Shiina (Bentham Science Publishers, 2011), Ch. 10.
[43] T. Fujii *et al.*, *in Progress in Ultrashort Intense Laser Science XI*, eds. K. Yamanouchi, C. H. Nam, and P. Martin (Springer), to be published.
[44] J. R. Vaill, D. A. Tidman, T. D. Wilkerson, and D. W. Koopman, Appl. Phys. Lett. **17**, 20 (1970); J. R. Greig *et al.*, Phys. Rev. Lett. **41**, 174 (1978); J. R. Woodworth, P. J. Hargis, L. C. Pitchford, and R. A. Hamil, J. Appl. Phys. **58**, 1382 (1984); T. Shindo, Y. Aihara, M. Miki, and T. Suzuki, IEEE Trans. Power Delivery **8**, 311 (1993); M. Miki, Y. Aihara, and T. Shindo, J. Phys. D **26**, 1244 (1993); M. Miki and A. Wada, J. Appl. Phys. **80**, 3208 (1996).
[45] M. McCarthy and G. K. Parks, Geophys. Res. Lett. **12**, 393 (1985).
[46] J. R. Dwyer *et al.*, Science **299**, 694 (2003).
[47] D. M. Smith, L. I. Lopez, R. P. Lin, and C. P. Barrington-Leigh, Science **307**, 1085 (2005).
[48] H. Tsuchiya *et al.*, Phys. Rev. Lett. **99**, 165002 (2007).
[49] J. R. Dwyer *et al.*, J. Geophys. Res. **113**, D23207 (2008).
[50] C. V. Nguyen, A. P. J. van Deursen, and U. Ebert, J. Phys. D: Appl. Phys. **41**, 234012 (2008).
[51] S. H. Lin, A. A. Villaeys, and Y. Fujimura, *in Advances In Multi-photon Processed And Spectroscopy* **16**, Ch. 3 (World Scientific, Singapore, 2004).
[52] T. Fujii, N. Goto, M. Miki, T. Nayuki, and K. Nemoto, Opt. Lett. **31**, 3456-3458 (2006).
[53] F. J. Mehr and M. A. Biondi, Phys. Rev. **181**, 264 (1969).
[54] A. Zhidkov and A. Sasaki, Phys. Rev. E **59**, 7085 (1999).
[55] R. Ackermann *et al.*, Appl. Phys. B **82**, 561 (2006).
[56] Y. Brelet *et al.*, Appl. Phys. Lett. **100**, 181112 (2012).
[57] M. Henriksson, J.-F. Daigle, F. Theberge, M. Chateauneuf, and J. Dubois, Opt. Express **20**, 12721 (2012).
[58] J.-F. Daigle *et al.*, Appl. Phys. Lett. **103**, 184101 (2013).
[59] R. S. Sigmond, J. Appl. Phys. **56**, 1355 (1984).
[60] T. Suzuki, J. Appl. Phys. **42**, 3766 (1971).
[61] S. Eto, A. Zhidkov, Y. Oishi, M. Miki, and T. Fujii, Opt. Lett. **37**, 1130 (2012).
[62] A. V. Gurevich, K. P. Zybin, and R. A. Roussel-Dupre, Phys. Lett. A **254**, 79 (1999).
[63] T. C. Marshall, M. P. McCarthy, and W. D. Rust, J. Geophys. Res. **100**, 7097 (1995).
[64] V. A. Saranin, Physics-Uspekhi **45**, 1287 (2002).
[65] CERN Program Library at http://geant4.web.cern.ch/geant4/
[66] R. Salamé *et al.*, Appl. Phys. Lett. **91**, 171106 (2007).
[67] G. Méjean *et al.*, Phys. Rev. E **72**, 026611 (2005).
[68] G. Méchain *et al.*, Appl. Phys. B **80**, 785 (2005).